ACS Catalysis

Research Article

pubs.acs.org/acscatalysis

Hydrogen Adsorption on Co Surfaces: A Density Functional Theory and Temperature Programmed Desorption Study

Pieter van Helden,*[,†] Jan-Albert van den Berg,[†] and Cornelis J. Weststrate[‡]

[†]Sasol Technology (Pty) Ltd., P.O. Box 1, Sasolburg, 1947 South Africa

[‡]Sasol Technology Netherlands B.V., Eindhoven University of Technology, P.O. Box 513, 5600 MB Eindhoven, The Netherlands

Supporting Information

ABSTRACT: Density functional theory (DFT) calculations and temperature programmed desorption (TPD) experiments were performed to study the adsorption of hydrogen on the Co(111) and Co(100) surfaces. On the Co(111) surface, hydrogen adsorption is coverage dependent and the calculated adsorption energies are very similar to those on the Co(0001) surface. The experimental adsorption saturation coverage on the Co(111)/(0001) surface is $\theta_{max} \approx 0.5$ ML, although DFT predicts $\theta_{max} \approx 1.0$ ML. DFT calculations indicate that preadsorbed hydrogen will kinetically impede the adsorption process as the coverage approaches $\theta = 0.5$ ML, giving rise to this difference. Adsorption on Co(100) is coverage independent up to $\theta = 1.00$ ML, contrasting observations on the Ni(100) surface. Hydrogen atoms have low barriers of diffusion on both the Co(111) and Co(100) surfaces. A microkinetic analysis of desorption, simulating the expected TPD experiments, indicated that on the Co(111) surface two TPD peaks are expected, while on the Co(100) only one peak is expected. Low coverage adsorption energies of between 0.97 and 1.1 eV are obtained from the TPD experiment on a smooth single crystal of Co(0001), in line with the DFT results. Defects play a important role in the adsorption process. Further calculations on the Co(211) and Co(221) surfaces have been performed to model the effects of step and defect sites, indicating that steps and defects will expose a broad range of adsorption sites with varying (mostly less favorable) adsorption energies. The effect of defects has been studied by TPD by sputtering of the Co crystal surface. Defects accelerate the adsorption of hydrogen by providing alternative, almost barrierless pathways, making it possible to increase the coverage on the Co(111)/(0001) surface to above $\theta = 0.50$ ML. The presence of defects at a high concentration will give rise to adsorption sites with much lower desorption activation energies, resulting in broad low temperature TPD features.

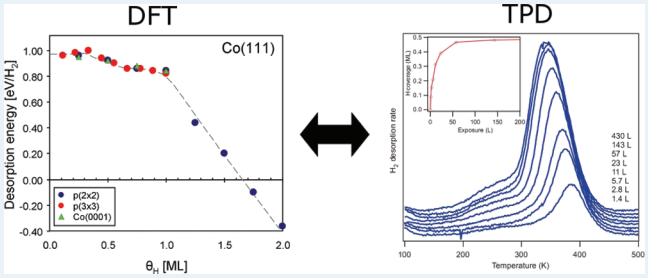

KEYWORDS: *DFT, TPD, hydrogen adsorption, microkinetic analysis, cobalt*

INTRODUCTION

The chemisorption of hydrogen on transition metal surfaces is of great interest in heterogeneous catalysis. Numerous transition metal surfaces catalyze hydrogenation reactions, which require the presence of adsorbed hydrogen atoms. Hydrogen chemisorption on cobalt surfaces is particularly important in processes such as the Fischer−Tropsch synthesis reaction.[1] Despite the prominence of the hydrogen chemisorption reaction on Co, it has not been extensively studied.

There are a number of experimental studies focusing on hydrogen chemisorption on Co.[2−6] On the Co(0001) surface,[2,3] it was shown that hydrogen adsorbs dissociatively, with a molecular adsorption energy of 0.76 ± 0.09 eV and an initial sticking probability of ≈0.04. Deuterium adsorption on Co(0001) gave rise to a faint (2 × 2) LEED pattern at low temperatures.[6] A deuterium saturation coverage of 0.64 ML deuterium atoms at 180 K was obtained. On Co thin films,[4,5] it was shown that hydrogen also adsorbs dissociatively, with a sticking probability close to unity. Two hydrogen adsorbed states are proposed, with the state below $\theta_H \approx 0.5$ ML having an adsorption energy of 0.89 ± 0.02 eV per hydrogen molecule.

The Ni(111) surface is closely related to Co(0001). Hydrogen on Ni(111) was studied in great depth by Rendulic et al.,[7,8] and it was noted that it can be expected that Co(111) should behave in a similar way as Ni(111). TPD studies[9−11] showed that on Ni(111) both the hydrogen desorption barrier and the desorption pre-exponential factor exhibit coverage dependent behavior, with the hydrogen desorption barrier decreasing slightly at half saturation coverage and then decreasing strongly as saturation coverage is approached.

A very limited number of theoretical studies of hydrogen adsorption on Co(0001) are available.[12,13] Klinke and Broadbelt[12] used non spin-polarized calculations to study hydrogen adsorption. The adsorbed hydrogen was considered for various high symmetry sites at only two, rather high, coverages (θ_H = 0.5 ML and θ_H = 1.0 ML). At both these coverages, the on top site adsorption was unfavorable. The calculated site stability has the order on top < subsurface < bridge < hcp hollow < fcc

Received: December 14, 2011
Revised: March 8, 2012
Published: April 18, 2012

   dx.doi.org/10.1021/cs2006586 | ACS Catal. 2012, 2, 1097−1107

hollow. The most stable hydrogen adsorption site at both 0.50 and 1.00 ML hydrogen coverages was the fcc hollow site, with adsorption energies of 0.48 and 0.46 eV per hydrogen atom, respectively. Despite only having calculated these two coverages, they proceeded to conclude that the hydrogen adsorption energy is not coverage dependent. Greeley and Mavrikakis[13] only considered hydrogen adsorption in the hcp and fcc hollow sites at θ_H = 0.25 ML with both the PW91 and RPBE exchange-correlation functionals. The PW91 zero-point vibration corrected adsorption energies for the fcc and hcp hollows sites were calculated to be 0.61 and 0.58 eV per atom, respectively. They proposed that the hydrogen diffusion at θ_H = 0.25 ML proceeds with a barrier of 0.16 eV. They also show that subsurface hydrogen adsorption at θ_H = 0.25 ML is endothermic and would therefore be unfavorable.

Turning our focus from single crystal surface science to relevant catalytic systems, it is important to consider the fact that many supported cobalt catalysts are usually synthesized to contain cobalt crystallites with average diameters less than 100 nm.[14] Cobalt crystallites with a diameter less than 100 nm are stable as FCC-Co (β).[15] The adsorption of hydrogen on the surfaces of FCC-Co is therefore of interest to us. Despite this bulk phase difference, the most dense surface planes that originate from both the HCP and FCC bulk phases (HCP-Co(0001) and FCC-Co(111), respectively) have the same hexagonal surface geometry with similar surface lattice parameters. The first structural difference between these two analogous surfaces lie only at the third Co layer. It is therefore reasonable to expect very similar surface adsorption energetics on both these most dense surfaces. There is also the possibility that the FCC-Co(100) surface is exposed in small crystallites. This surface has a square surface geometry. The specific atomic arrangement of this surface cannot be generated from a low Miller index cut through the HCP-Co bulk.

In an attempt to provide insight into the adsorption of hydrogen on Co surfaces, this paper considers the results of temperature programmed desorption (TPD) experiments on a single crystal exposing the Co(0001) surface. The TPD experiments consider the surface with and without the presence of defect sites. Furthermore, theoretical calculations were used to study hydrogen adsorption structures on the Co(111) and Co(100) surfaces (as well as a comparison on the calculated Co(0001) surface) within the spin-polarized pseudopotential approximation of first principles density functional theory. Further calculations on the Co(211) and Co(221) stepped surfaces were considered as models for defect site adsorption. The calculated results are compared to the singel crystal TPD experiments.

METHODS AND MODELS

Experimental Procedures. Thermal desorption of hydrogen was studied in a vacuum system equipped with a LEED/Auger system, a quadrupole mass spectrometer, and a sputter gun for sample cleaning. The base pressure of this system is 1×10^{-10} mbar. The disk-shaped sample (diameter 8 mm) was clamped between tungsten wires, which were used for heating (direct current) and cooling the sample. The cobalt single crystal was cleaned by repeated cycles of Ar+ sputtering (3.3 kV, 5 min) at 630 K and annealing in vacuum at 630 K for 30 min. Auger and LEED indicated a clean, smooth HCP-Co(0001) surface afterward. A synchrotron XPS study performed on the same sample revealed that the applied cleaning procedure yields a clean Co surface.[16] Thermal desorption of CO and hydrogen also indicated a clean surface, and the obtained desorption traces were identical to those reported in literature.[6,17] To quantify the amount of desorbing hydrogen, decomposition of methanol was used, as it decomposes into CO and H_2.[18] The resulting CO desorption was calibrated using the known coverage of CO at 340 K (1/3 ML)[17] and the corresponding amount of hydrogen deduced from the CO:H ratio in methanol. The hydrogen doses reported here were calculated using an ion gauge sensitivity factor of 0.35.

Computational Methods. The quantum chemical calculations in this study were performed using the Vienna ab initio simulation package (VASP).[19,20] This code uses periodic DFT with a plane wave basis set and pseudopotentials. We used the spin-polarized generalized gradient approximation (GGA) with the Perdew and Wang exchange-correlation functional (PW91)[21] with ultrasoft pseudopotentials. The electron distribution at the Fermi level was modeled by the approach proposed by Methfessel and Paxton[22] with σ = 0.2 eV. A five-layer slab was used for the Co(111) and the Co(0001) surfaces and a four layer slab was used for the Co(100) surface. The surfaces were represented by using $p(2 \times 2)$ and $p(3 \times 3)$ surface unit cells. These models have a 10 Å vacuum layer between the repeating surfaces. Apart from the constrained bottom two layers of both slabs, all the atoms in the configurations were allowed to relax upon optimization. The *k*-point sampling was generated by following the Monkhorst–Pack[23] procedure with $9 \times 9 \times 1$ and $5 \times 5 \times 1$ meshes for the Co(111) and Co(0001) surfaces and $5 \times 5 \times 1$ and $4 \times 4 \times 1$ meshes for the Co(100) surfaces. The plane wave basis set cutoff energy was set at 400 eV. The stepped Co(211) and Co(221) surfaces were represented by using $p(1 \times 2)$ surface unit cells. A four-layer slab was used for the Co(211) and a five-layer slab was used for the Co(221) surface. In both cases, the bottom layer of atoms was constrained. The *k*-point sampling was performed with a $6 \times 7 \times 1$ mesh for Co(211) and $7 \times 5 \times 1$ mesh for Co(221).

By fitting various bulk Co cells to the Birch–Murnaghan equation of state,[24,25] we obtained the equilibrium lattice constant and bulk modulus. For bulk FCC Co, a lattice parameter of 3.538 Å was obtained. This structure has a bulk modulus of 202 GPa and a magnetic moment of 1.67 μ_B per Co atom. These values are in good agreement with the experimental values of bulk FCC Co (3.550 Å,[26] 191 GPa,[27] and 1.70 μ_B,[28] respectively). Corrected average surface energies (according to the procedure of Mattson and Mattson[29]) of 2.79 and 3.20 J·m^{-2} were obtained for the Co(111) and Co(100) slabs, respectively. These are in the same range as the experimental estimate of 2.52 J·m^{-2}.[30] For bulk HCP Co, lattice parameters of 2.503 and 4.062 Å were obtained. This structure has a bulk modulus of 204 GPa and a magnetic moment of 1.62 μ_B per Co atom. These values are in good agreement with the experimental values of bulk HCP Co (2.507 and 4.061 Å,[31] 199 GPa,[32] and 1.72 μ_B,[30] respectively).

The gas-phase H_2 molecule was calculated by placing the molecule in a cubic unit cell with 10 Å sides. The equilibrium bond distance (r_e) was determined to be 0.749 Å, together with a vibrational frequency of ν = 4400 cm^{-1}. These agree well with the experimental values of r_e = 0.741 Å and ν = 4401 cm^{-1}.[33]

The adsorption of hydrogen has been considered on a single side of the Co surface slabs. Dipole corrections have been applied in the calculations to avoid artificial dipole effects. Partial Hessian vibrational analyses were performed on the

optimized hydrogen atoms in the resulting structures. The resulting zero-point vibrational corrections were included in the adsorption energies. The adsorption energies (E_{ads}) per hydrogen atom on the considered surface were calculated with respect to the relaxed clean slabs (E_{slab}) and an isolated hydrogen molecule (E_{H_2}):

$$E_{ads} = \frac{1}{x}\left(E_{(slab+xH)} - E_{slab} - \frac{x}{2}E_{H_2}\right) \quad (1)$$

with x being the number of hydrogen atoms in the unit cell. To take into account, the effects of coverage we sequentially introduced hydrogen atoms into the cell. In this study, we limit ourselves to consider only hydrogen atoms adsorbed on the Co surface.

Constrained optimization and the VASP implementation of the nudged elastic band (NEB) method[34] were used to develop adsorption profiles and locate transition states.

Microkinetic analysis was used to simulate the TPD spectra. This analysis was performed with the in-house developed *kinsolv* code for the integration of reaction rate equations. The rate constant (k) for hydrogen desorption was estimated from transition-state theory.[35,36] The implementation of the *kinsolv* code incorporates the explicit use of coverage dependent activation energies in the estimation of the rate constant. The TPD signal is proportional to the rate of desorption and therefore the simple rate expression for hydrogen desorption was used:

$$\frac{d[H_2]}{dt} = -\frac{d\theta_H}{dt} = k(\theta_H)\theta_H{}^2 \quad (2)$$

The rate constant can be expressed in terms of the entropy ($\Delta S^{\ddagger}$) of activation and the coverage dependent activation enthalpy ($\Delta H^{\ddagger}(\theta_H)$):

$$k(\theta_H) = \frac{k_B T}{h} e^{\Delta S^{\ddagger}/R} e^{-\Delta H^{\ddagger}(\theta_H)/RT} \quad (3)$$

where k_B is the Boltzmann constant, T the temperature, R is the gas constant, and h the Planck constant. The coverage dependent activation enthalpy function of the reaction can be estimated from the calculated coverage dependent zero-point corrected DFT desorption energies. Our experimental observations (vide infra) for partially annealed systems (where a small amount of defect sites are present) show adsorption of hydrogen to rapidly proceed to above 0.5 ML coverage due to the existence of low-barrier adsorption pathways. To generate microkinetic TPD simulations of the Co(111) surface, in which the coverage exceeds 0.5 ML, required the assumption of such a low-barrier process for adsorption. Since the adsorption barrier will be small compared to the desorption energy we use only the calculated desorption energies to estimate the activation energy of the desorption process. To obtain a smooth function from the DFT desorption energy values the *kinsolv* code interpolates the DFT results by means of a Lagrange polynomial. The entropic contribution is estimated by using the relevant partition function contributions for the low coverage adsorbed and transition states. The desorption transition state is assumed to be a free 2D H_2 gas. As a first attempt it was assumed that the entropic contribution of the adsorbed state is coverage independent, but still a function of temperature:

$$S_{ads}(T) = R \ln[q_{vib}(T) q_{trans}(T)] \quad (4)$$

where $q_{vib}(T)$ is the vibrational partition function and $q_{trans}(T)$ is the 2D translational partition function, incorporating the diffusion of the adsorbed hydrogen atom. Details of these functions can be seen in the Supporting Information.

EXPERIMENTAL RESULTS

Desorption from a Smooth Surface. Figure 1 summarizes the thermal desorption results (2 K/s) that were obtained after dosing hydrogen at 100 K on the clean, well-annealed Co(0001) surface. The inset shows the hydrogen coverage as a function of exposure. The spectra show a single, broad peak with a peak temperature varying from 390 K for low coverage to 350 K for a saturated surface, the peak shift being indicative of a second order desorption process. Quantification (using methanol decomposition as described in the experimental part) gives a saturation coverage of 0.45−0.50 ML hydrogen atoms. A faint (2 × 2) LEED pattern was found after saturation at 100 K. The initial sticking coefficient estimated from the uptake curve is 0.01−0.05. This is in agreement with previous sticking probability estimations.[2] Our results are in agreement with the earlier reported D_2 desorption spectrum from Co(0001).[6] Quantification of their desorption traces yielded a D_2 saturation coverage, at 180 K, of θ = 0.27 ML, i.e. θ = 0.54 ML of deuterium atoms, slightly higher than the value we report here. Those authors also reported a faint (2 × 2) LEED pattern can be observed at lower temperature.

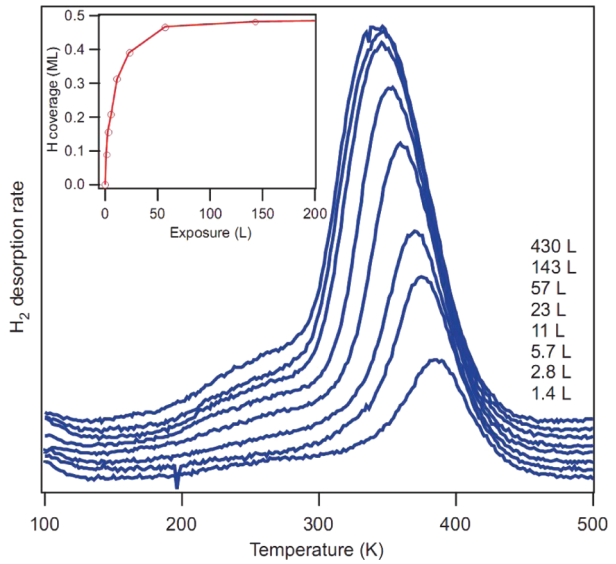

Figure 1. Hydrogen desorption from a smooth Co(0001) surface for different hydrogen doses. (inset) Corresponding hydrogen adsorption uptake curve.

Various analysis methods can be employed to obtain the low coverage desorption activation energies and pre-exponential factors from the TPD traces. The first simple approach is to use a second-order Arrhenius plot in which the $\ln(rate_{max}/\theta^2)$ is plotted against $1/T_{max}$. This approach gives a straight line from which a desorption barrier of 0.71 ± 0.12 eV/H_2 was obtained. This value corresponds well to the value reported by Bridge et al.,[2] although it is much lower than the low coverage values calculated by DFT (vide infra). We have proceeded to use additional analyses, including the second-order Redhead[37] method using an assumed pre-exponential factor of 10^{13} $ML^{-1}\cdot s^{-1}$, which is close to typical values of k_BT/h at the

dx.doi.org/10.1021/cs2006586 | ACS Catal. 2012, 2, 1097−1107

considered desorption peak temperatures. Furthermore, we applied the leading edge analysis,[38] as well as the method of analysis proposed by Falconer and Madix.[39] The resulting values can be seen in Table 1. The desorption activation

Table 1. Desorption Activation Energies per H_2 Molecule (E_d) and Pre-exponential Factors (ν) Extracted from the Low Coverage TPD Traces on Co(0001)

analysis method	θ	E_d [eV]	ν [$ML^{-1}\cdot s^{-1}$]
simple Arrhenius plot		0.71 ± 0.12	
Redhead[37]	0.08	0.97	10^{13} [a]
	0.00[b]	0.98	10^{13} [a]
leading edge analysis[38]	0.08	1.07 ± 0.02	$10^{11.26\pm0.06}$
Falconer and Madix[39]	0.00[b]	1.10 ± 0.18	$10^{10.70\pm1.31}$
lit. Co(0001)[2c]		0.76 ± 0.14	
lit. Co films[4,5]	<0.50	0.89 ± 0.04	
DFT Co(111)	0.11	0.97	

[a]Assumed value used in analysis. [b]Extrapolated to 0.00 ML coverage. [c]Simple Arrhenius plot was used.

energies given by these three methods vary from 0.97 to 1.1 eV. These values are higher than those proposed from previous experiments, but they are in very good agreement with the low coverage DFT values (0.97 eV at θ = 0.11 ML and 0.95 eV at θ = 0.25 ML)(vide infra). These values are also in line with the low coverage desorption activation energy on Ni(111) of between 0.95 and 1.00 eV.

Influence of Defects. To investigate the influence of defects on the hydrogen adsorption and desorption on Co(0001), the following experiment was performed: the well-annealed surface was exposed to hydrogen at 100 K, after which desorption was recorded. Then, the surface was sputtered for a short time (1 min, 3.3 keV, 300 K), after which it was exposed to the same dose of hydrogen at 100 K. After that, the desorption was recorded, up to 500 K. The sample temperature was kept at 500 K for 24 s, which led to partial annealing of the surface defects due to the sputtering treatment (hereafter called the partially annealed surface). Then, the hydrogen adsorption and desorption was repeated, using the same H_2 dose. It is very difficult to measure the concentration of defects on the surface. With the above type of treatments, results can be obtained in two scenarios: a "high" defect concentration scenario (sputtered surface) and a "low" defect concentration scenario (partially annealed surface). The result of this experiment, for several hydrogen doses, is shown in Figure 2.

The desorption traces found for the sputtered surface after saturation with hydrogen (570 L) differs greatly from that of the annealed surface: The saturation coverage is up to θ = 0.75 ML, and the hydrogen desorbs in two broad peaks, one centered at 220 K (β_1) and the other at 310 K (β_2), both at significantly lower temperatures than the single desorption peak (β_2) from the smooth surface, which is centered around 340 K and is equivalent to θ = 0.5 ML. The desorption spectrum of the partially annealed surface shows the same adsorptions peak as the well-annealed (smooth) surface, but in addition to this peak (β_2) at 340 K a shoulder is observed, centered at 295 K (β_1). The total amount of hydrogen that adsorbs on this surface is θ = 0.61 ML.

The results for lower hydrogen doses reveal interesting information about the H_2 adsorption process. The sputtered surface is already saturated with a coverage of θ = 0.75 ML after a dose of 5.7 L, while on the smooth surface, this dose produces

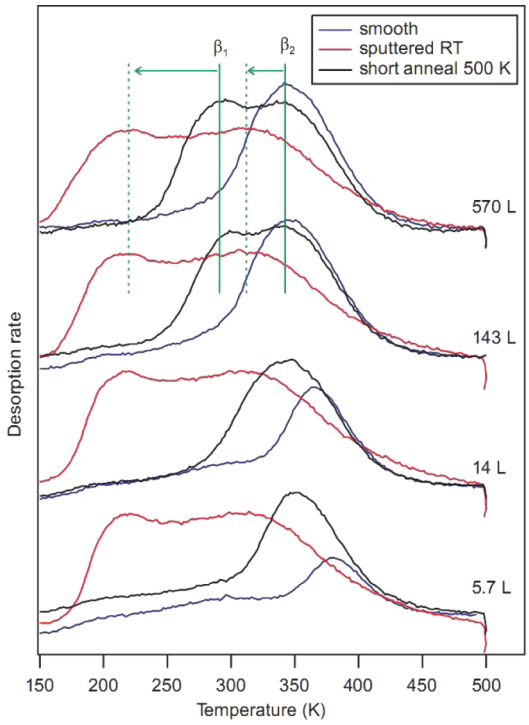

Figure 2. Hydrogen desorption from a smooth, a slightly defected (sputtered and annealed), and a heavily defected surface (sputtered) for different hydrogen doses.

a subsaturated layer with a coverage of 0.1 ML. On the partially annealed surface, the same dose of hydrogen produces a coverage of θ = 0.35 ML. For the intermediate doses of 14 and 143 L, the hydrogen coverage on the smooth surface continues to increase, reaching a saturation after a dose of 143 L (see also the inset of Figure 1 and ref 6). For the partially annealed surface, the (β_2) peak fills up more quickly than on the smooth surface, and at higher doses the (β_1) state gets populated. This state is not saturated after a dose of 143 L, suggesting that the sticking coefficient of hydrogen has dropped significantly after the β_2 state has been filled. These experiments show that hydrogen sticking is strongly enhanced by defects and they allow other hydrogen adsorption states to be populated, which are experimentally inaccessible on the smooth surface. In this way, the defects facilitate a higher saturation coverage.

■ COMPUTATIONAL RESULTS

The chemisorption calculations of hydrogen on the FCC Co(111) and Co(100) surfaces have been performed using four sets of calculations. The first two sets have been done by calculating the adsorption structures of hydrogen on the available high symmetry sites in the respective $p(2 \times 2)$ surface unit cells. These results will be discussed in the first section. The following set contains all the most stable adsorption orientations in the respective $p(3 \times 3)$ surface supercells for coverages ranging from θ = 0.11 ML to higher than θ = 1.00 ML. We use data from these sets to construct coverage dependent adsorption energy profiles for the two fcc surfaces. In this section, we will present simulated TPD profiles constructed with a microkinetic simulation using the calculated coverage dependent data. We also consider the effect of a precoverage of hydrogen on the adsorption process and make a first attempt to model the effects of steps and defect sites.

dx.doi.org/10.1021/cs2006586 | ACS Catal. 2012, 2, 1097–1107

Hydrogen Adsorption Sites. The resulting energetic and geometric parameters for the hydrogen adsorption configurations on various sites of the $p(2 \times 2)$ surface unit cells of Co(111) and Co(100) are given in Tables 2 and 3, respectively. The sites exposed by these two surfaces can be seen in Figure 3. The reported results in these tables are functions of the coverage and specific surface sites.

Table 2. Zero-Point Energy Corrected Adsorption Energies (E_{ads}) of Hydrogen Adsorption Structures at Various Coverages (θ) in the $p(2 \times 2)$ Co(111) Surface Supercell[a]

θ [ML]	site[b]	E_{ads} [eV]	E_{ads}'[c] [eV]	Z_H[d] [Å]	ν_i[e] [cm^{-1}]
0.25	OT	0.09	0.08	1.52	1747, 271*i*, 343*i*
	BR	−0.36	−0.36	1.08	1242, 1100, 478*i*
	HH	−0.47	−0.46	0.97	1088, 833, 802
	FH	−0.48	−0.48	0.97	1178, 861, 826
0.50	OT	0.20	0.19	1.47	1786, 1776, 448, 271*i*, 333*i*, 395*i*
	BR	−0.38	−0.38	1.08	1305, 1299, 1192, 937, 381*i*, 433*i*
	HH	−0.44	−0.45	0.94	1156, 1135, 995, 842, 793, 734
	FH	−0.46	−0.46	0.93	1187, 1145, 1030, 928, 744, 727
0.75	OT	0.28	0.28	1.45	1868, 1821, 1787, 485, 242, 155, 284*i*, 416*i*, 451*i*
	BR	−0.27	−0.27	1.07	1325, 1302, 1252, 1230, 1173, 911, 88, 393*i*, 607*i*
	HH	−0.43	−0.43	0.91	1188, 1183, 1111, 970, 952, 894, 822, 814, 748
	FH	−0.43	−0.44	0.90	1214, 1193, 1177, 985, 981, 957, 897, 892, 866
1.00	OT	0.35	0.34	1.50	1893, 1891, 1888, 1851, 414, 395, 357, 273*i*, 343*i*, 360*i*, 394*i*, 455*i*
	BR	−0.21	−0.22	1.05	1340, 1315, 1315, 1251, 1178, 1170, 879, 792, 403, 184*i*, 389*i*, 654*i*
	HH	−0.41	−0.41	0.91	1185, 1161, 1152, 1146, 1022, 1003, 969, 956, 946, 895, 824, 788
	FH	−0.42	−0.42	0.91	1211, 1167, 1154, 1150, 1057, 1045, 1002, 985, 977, 934, 860, 809

[a]Calculated adsorption energies on the Co(0001) surface (E_{ads}') are given for comparison. [b]Site labels: (on-top) OT; (bridge) BR; (fcc hollow) FH; (hcp hollow) HH. [c]Details of the Co(0001) adsorption structures are given in the Supporting Information. [d]The average height above the Co surface. [e]Lists the calculated vibrational frequencies.

Hydrogen Adsorption on Co(111). At the coverage of θ = 0.25 ML on Co(111), it is clear that the adsorption in the hcp and fcc hollow sites have no imaginary vibrational frequencies and are thus the only local minima structures on the potential energy surface (PES), with adsorption energies of −0.47 and −0.48 eV, respectively. Of these two, adsorption in the fcc hollow site is more stable by 0.01 eV. The adsorption energy of −0.48 eV is similar to that of the low coverage regime of the structurally analogous Ni(111) surface (between −0.47 and −0.50 eV).[11] The structure with hydrogen adsorbed on the on-top site has two imaginary frequencies. This indicates that this structure is located at a second-order saddle point on the PES. The adsorption energy is also positive indicating that it is not stable compared to the gas phase hydrogen molecule. The preferred adsorption site order for the Co(111) surface presented here is the same as that proposed by Klinke and

Table 3. Zero-Point Energy Corrected Adsorption Energies (E_{ads}) of Hydrogen Adsorption Structures at Various Coverages (θ) in the $p(2 \times 2)$ Co(100) Surface Supercell

θ [ML]	site[a]	E_{ads} [eV]	Z_H[b] [Å]	ν_i[c] [cm^{-1}]
0.25	OT	0.01	1.52	1732, 69, 257*i*
	BR	−0.33	1.11	1269, 1089, 331
	H	−0.46	0.69	796, 662, 470
0.50	OT	0.05	1.52	1809, 1749, 2534, 56*i*, 201*i*, 282*i*
	BR	−0.33	1.09	1314, 1289, 1154, 848, 419, 360
	H	−0.46	0.64	757, 708, 663, 547, 486, 348
0.75	OT	0.17	1.50	1847, 1834, 1771, 431, 274, 173*i*, 218*i*, 258*i*, 283*i*
	BR	−0.27	1.07	1304, 1282, 1277, 1156, 1072, 873, 637, 391, 293
	H	−0.45	0.58	827, 798, 764, 761, 713, 690, 609, 432, 389
1.00	OT	0.23	1.50	1852, 1838, 1836, 1836, 392, 311, 198, 150, 182*i*, 293*i*, 294*i*, 349
	BR	−0.24	1.08	1332, 1309, 1289, 1270, 1160, 1143, 923, 797, 650, 629, 440, 247
	H	−0.45	0.52	913, 830, 798, 788, 759, 712, 712, 692, 658, 624, 511, 445

[a]Site labels: (on-top) OT; (bridge) BR; (hollow) H. [b]The average height above the Co surface. [c]Lists the calculated vibrational frequencies.

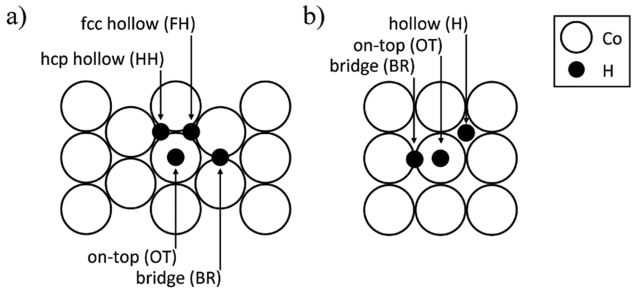

Figure 3. High symmetry adsorption sites on (a) Co(111)/Co(0001) and (b) Co(100).

Broadbelt on the Co(0001) surface.[12] The structure with hydrogen adsorbed on the bridge site has only one imaginary frequency. This indicates that it is a transition state, and in this case, it is the transition state for diffusion. The resulting calculated low coverage diffusion barrier for hydrogen on Co(111) is 0.12 eV. This is similar to the values on the Co(0001) surface previously proposed by other authors.[12,13] The consequence of this low barrier is that the hydrogen atom will be very mobile on the surface at realistic catalytic temperatures. Furthermore, the mobility of hydrogen atoms on the Co surface is similar to the high mobility observed experimentally on Ni(111).[40]

As the coverage increases, it is clear that the fcc and hcp hollow sites remain the only two local minima on the PES up to θ = 1.00 ML. The other two sites give rise to higher-order saddle points at all the considered coverages above θ = 0.25 ML. In this whole range the fcc hollow site configurations are in each case only slightly more stable than the hcp hollow sites. As the coverage increases from θ = 0.25 to 1.00 ML, the adsorption energies of the fcc and hcp hollow sites both decrease by 0.06 eV per hydrogen atom. This will correspond to a decrease in the H_2 desorption energy of 0.12 eV.

Comparison of Hydrogen Adsorption on the Co(111) and Co(0001) Surfaces. As we have noted, the Co(0001) and

dx.doi.org/10.1021/cs2006586 | ACS Catal. 2012, 2, 1097−1107

Co(111) surfaces have the same hexagonal surface structure, with the first structural difference arising only at the third Co layer. Similar surface adsorption energetics can therefore be expected on both these most dense surfaces. If the calculated adsorption energies on these two surfaces are compared (see Table 2), it is clear that the values are indeed very similar. Overall, the average of the difference between the energies is 0.01 eV, with the largest single difference being 0.03 eV. Since the energies and the trends in the energies are similar on both these high density hexagonal surfaces, we can therefore regard them as being exactly the same. This validates the comparisons between the Co(111) DFT results and the experimental results on Co(0001) presented in this paper.

Hydrogen Adsorption on Co(100). The resulting hydrogen adsorption energies on the Co(100) surface can be seen in Table 3. At a coverage of θ = 0.25 ML, the adsorption of hydrogen in the hollow and on the bridge sites both result in local minima structures on the PES, with adsorption energies of −0.46 and −0.33 eV, respectively. Despite the fact that the Co(100) surface is more open than the Co(111), the Co(100) hollow site adsorption energy is not larger, but almost the same as the values on Co(111). This is similar to the similarity in adsorption energies for Ni(111) and Ni(100) surfaces in Figure 4. In a twofold structure, very close to the bridge site lies the transition state of diffusion to the hollow site. The energy difference between the bridge site and this transition state is negligible. This results in a hydrogen diffusion barrier of 0.14 eV at low coverage. This indicates that the hydrogen atom will also be very mobile on this surface at relevant catalytic temperatures. The on-top site has an imaginary frequency, indicating that this structure is located at a saddle point on the PES. Furthermore, the adsorption energy is positive, indicating that it is not stable compared to the gas phase hydrogen molecule. As the hydrogen coverage increases to θ = 1.00 ML, both the hollow and bridge sites remain local minima on the PES, while the on-top hydrogen structures are higher-order saddle points. The hollow site remains the most stable adsorption structure throughout, with the adsorption energy changing by only 0.01 eV over the whole range.

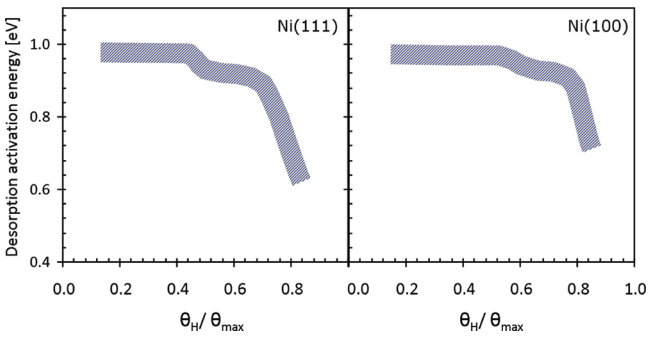

Figure 4. Hydrogen desorption activation energies for the Ni(111) and Ni(100) surfaces. Adapted from the work of Zhdanov.[11] Original data were by Seebauer et al.[9,10].

Coverage Dependence of Hydrogen Adsorption. By extending the presented data on the $p(2 \times 2)$ surface supercells to coverages higher than θ = 1.00 ML and combining it with further calculation in $p(3 \times 3)$ surface supercells, detailed coverage dependent hydrogen adsorption profiles can be generated for both the Co(111) and Co(100) surfaces. The resulting coverage dependent profiles are shown in terms of H_2 desorption energies in Figure 5. Details of most stable calculated structures can be found in the Supporting Information.

For Co(111) it is clear that hydrogen adsorption and desorption will be hydrogen coverage dependent. Although there is an initial small stabilization up to θ = 0.33 ML, the desorption energy decreases by a significant amount in the region between θ = 0.33 and 0.7 ML. This is similar to what has been shown on Ni(111)[11] (see Figure 4). Once the hydrogen coverage is increased to above θ = 1.00 ML the average desorption energy decreases rapidly in a linear fashion. A rough estimate of the maximum saturation coverage of $\theta_{max} \approx$ 1.00 ML has been obtained from the differential desorption energy. This is larger than the initially observed experimental saturation coverage ($\theta \approx$ 0.50 ML) on a smooth Co(0001) surface (vide supra). If the decrease in adsorption strength as coverage increases is correctly represented by this DFT model, we can expect an approximate decrease in the desorption peak temperature of around 46−60 K if the coverage can be increased to θ = 1.00 ML (see the Supporting Information for the calculation).

For Co(100), the calculations suggest that hydrogen adsorption and desorption will be less affected by the hydrogen coverage below θ = 1.00 ML. The desorption energy remains almost constant up to θ = 1.00 ML with an average value of 0.91 ± 0.02 eV (maximum decrease from initial value of 0.01 eV). This differs from what has experimentally been shown on

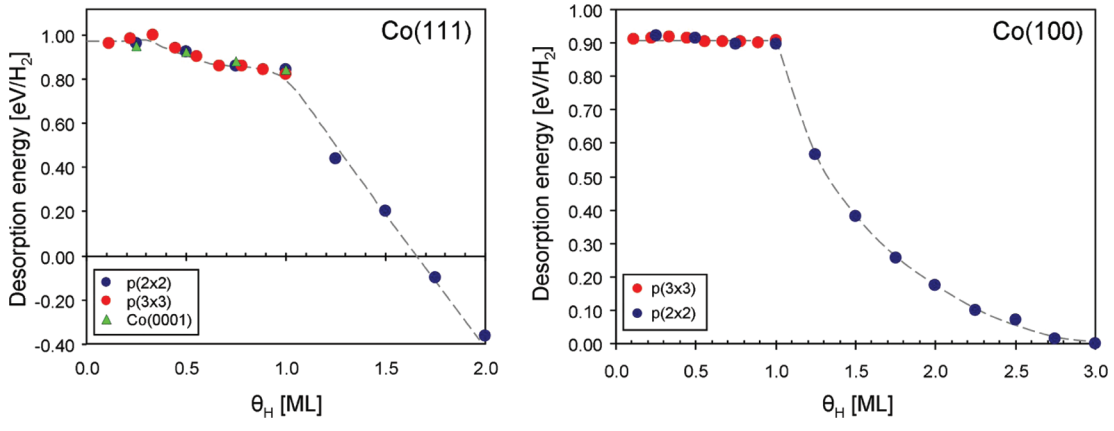

Figure 5. Coverage dependent H_2 desorption energies on the Co(111) and Co(100) surfaces. Dashed lines are only guides.

dx.doi.org/10.1021/cs2006586 | ACS Catal. 2012, 2, 1097−1107

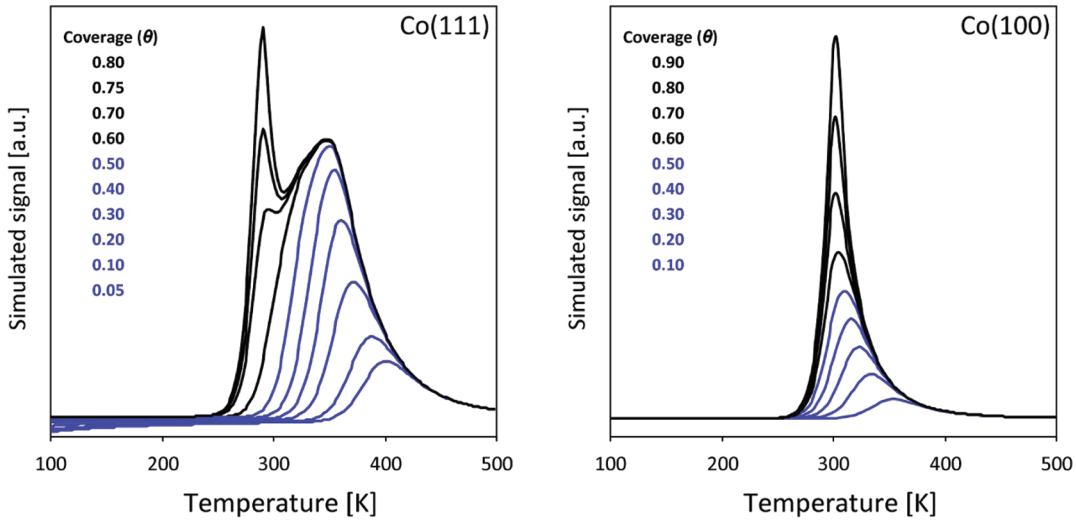

Figure 6. Simulated TPD profile for H_2 desorption on the Co(111) (left) and Co(100) (right) surfaces.

Ni(100)[11] (see Figure 4), where an average decrease of about 0.04 eV can be seen at around θ/θ_{max} = 0.6 ML. Once the hydrogen coverage is increased to above θ = 1.00 ML, the average desorption energy decreases significantly. A rough estimate of the maximum saturation coverage of $\theta_{max} \approx 1.00$ ML has been obtained from the differential desorption energy.

These coverage dependent profiles were used to simulate the expected TPD profiles on both the Co(111) and Co(100) surfaces. The resulting simulated TPD spectra can be seen in Figure 6. The simulated TPD desorption spectrum on the Co(111) surface shows one feature up to a coverage of 0.6 ML and two features at high coverage. At a coverage of θ = 0.05 ML, the desorption peak maximum lies at a temperature of 400 K. This is in good agreement with our TPD experiment (see Figure 1) where the low coverage peak lies at about 390 K. As is the case for second-order desorption, the peak maximum shifts to a lower temperature as the coverage increases. At θ = 0.50 ML, the desorption peak maximum lies at 350 K. This is once again in good agreement with our TPD experiment, where at close to θ = 0.50 ML the desorption peak maximum lies at about 340 K. As we increase the initial coverage to values higher than 0.50 ML, a second desorption feature arises at 290 K, corresponding well with the experimental β_1 feature shown in Figure 2 centered on 295 K. The temperature difference between he two simulated features at high coverage is 57 K. This temperature difference corresponds well with our simple prediction using the Redhead model giving a peak separation of between 46 and 60 K, and to our further TPD experiments (shown in Figure 2) where the difference between the β_1 and β_2 features is 55 K. Although the temperature shifts correspond quite well, the shape of the first feature is much sharper than the broad peak observed in the TPD experiment. This is due to the fact that in our microkinetic analysis we assumed that the low coverage vibrational and translational partition function can be used at all coverages, although we can expect it to be coverage dependent, as is the case for Ni(111).[11] A broader peak shape might be obtained if coverage dependent desorption entropies are included. We conclude that the origin of the second feature and the amount at which the peak maximum is shifted compared to the low coverage peak is due to the coverage dependent adsorption energies of hydrogen on the Co(111) surface.

Only one feature appears in the Co(100) simulated TPD spectrum. This is consistent with the calculated values that indicated no change in adsorption energy with an increasing coverage up to 1 ML on this surface. The low coverage (0.1 ML) peak maximum lies at 354 K, which is lower than on the Co(111) surface. The peak maximum shifts to a value of 302 K at the high coverage of θ = 0.90 ML.

Hydrogen Adsorption Pathways on Co(111). In understanding the adsorption of hydrogen on Co surfaces, it is also necessary to gain insight into the mechanism of the adsorption process, since this can have an impact on the observed saturation coverage. The minimum energy pathways for the hydrogen adsorption process on a clean surface was considered for a range of possible adsorption and dissociation sites. A selection of the most important pathways can be seen in Figure 7. In this process the H_2 molecule starts at 4 Å above the surface in a $p(2 \times 2)$ Co(111) unit cell with the H_2 bond parallel to the surface. As the H_2 molecule is brought closer to the surface, the changes in the system energy are noted. The pathway with the lowest overall barrier has the H_2 dissociating over the top site (blue curve in Figure 7), and the resulting

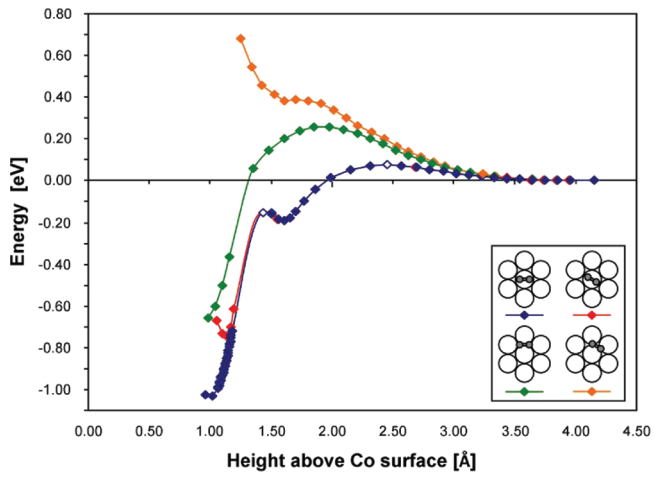

Figure 7. Minimum energy pathways for H_2 dissociation on a selection of sites on a clean Co(111) surface. The lowest energy TS structures are shown by open diamonds.

dx.doi.org/10.1021/cs2006586 | ACS Catal. 2012, 2, 1097–1107

hydrogen atoms move toward the corresponding hcp and fcc hollow sites. The energy profile of this pathway as a function of the height above the Co(111) surface can be seen in both Figures 7 and 8. It is interesting to note that as the molecule

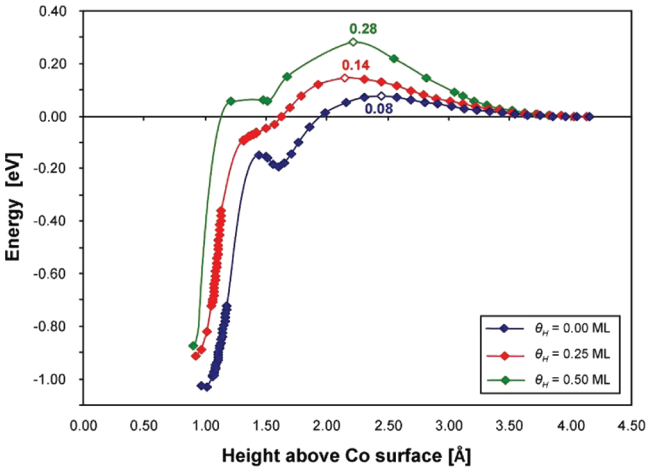

Figure 8. Minimum energy pathways for H_2 dissociation on clean and H-precovered Co(111) surfaces at various initial H coverages. In all cases the H_2 dissociates over the top site and moves toward the corresponding hcp and fcc hollows.

following this pathway approaches the surface, the energy of the system increases and reaches a maximum value of 0.08 eV at about 2.45 Å above the surface. After this barrier, the energy decreases as the molecule nears the surface until a small, molecularly adsorbed, exothermic minimum is reached at about 1.60 Å above the surface. From this minimum, only a small increase in the energy is required (0.04 eV) to dissociate the hydrogen molecule at about 1.5 Å above the surface. The highest point in this profile is the repulsive approach barrier.

This process was repeated in the presence of a single preadsorbed hydrogen atom in the cell to simulate the effect of an initial hydrogen coverage of θ = 0.25 ML. Similarly, we further considered this pathway with an initial coverage of θ = 0.50 ML. The resulting energy profiles for these two cases can be seen in Figure 8. As the precoverage of hydrogen is increased the approach barrier of the hydrogen molecule also increases. In the θ = 0.25 ML preadsorbed case, the approach barrier increased to 0.14 eV. The effect of this would correspond to a decrease in the adsorption rate by approximately four orders of magnitude at a typical adsorption experiment temperature of 100 K (see the Supporting Information for the kinetic expressions). At a precoverage of θ = 0.50 ML, the further increase in the barrier height would correspond to a decrease in the adsorption rate by another four orders of magnitude, thereby effectively inhibiting the adsorption process. This relates well to the experimental observation of a saturation coverage of $\theta \approx$ 0.50 ML on a smooth Co(0001) surface at 100 K (vide supra). This decrease in rate would not be as severe at higher temperatures. To be able to adsorb hydrogen up to θ = 1.00 ML, higher temperatures or alternative pathways (such as at steps and defects) would be required.

Hydrogen Adsorption on Stepped Surfaces. As was noted above, the less dense square Co(100) surface (metal coordination number CN = 8) has only a slightly smaller adsorption energy compared to the hexagonal high density Co(111) surface (CN = 9). The fact that an increase in the number of Co−H bonds did not increase the strength of hydrogen adsorption indicates that the hydrogen atom prefers not to be overcoordinated. In this case hydrogen prefers a hexagonal arrangement of Co atoms instead of a fourfold arrangement. If, as on actual catalytic crystallites, there are defect and stepped sites present, the arrangement and coordination numbers of the sites will differ from that of the Co(111) surface. As a first attempt to consider the effects of defect and stepped sites, we considered the adsorption of a single hydrogen atom on both the $p(2 \times 1)$ Co(211) and $p(1 \times 2)$ Co(221) stepped surfaces, resulting in low coverage hydrogen adsorption structures on these stepped surfaces. The surface structures of the Co(211) and Co(221) surfaces with their corresponding site labels can be seen in Figure 9. We

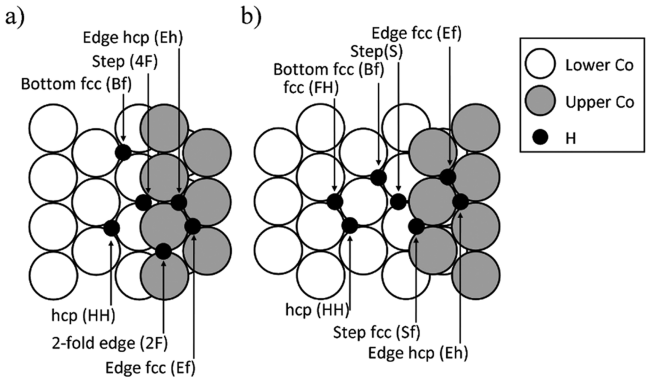

Figure 9. Considered adsorption sites on the (a) Co(211) and (b) Co(221) stepped surfaces.

consider these surfaces as models for surfaces with a heterogeneous arrangement of adsorption sites, each with a variety of Co coordination numbers typical of defect and step sites. It must be noted that the changes in adsorption energies we present will be at low hydrogen coverage. If the coverage is increased, it is likely that the lateral repulsions between hydrogen atoms (as shown on the Co(111) surface) can further decrease the adsorption energies. The resulting adsorption energies and the TPD peak temperatures estimated with the second-order Redhead equation[37] can be seen in Table 4. The estimated desorption temperatures on the Co(211) and Co(221) surfaces differ significantly as the adsorption site is varied. The Co(211) surface has estimated desorption peak temperatures varying from 252 to 395 K. On the Co(221) surface, the estimated TPD peaks temperatures vary from 237 to 430 K. A combination of these ranges fits well with the broad range of the desorption peaks shown in the TPD experiment on a heavily sputtered surface (see Figure 2). This indicates that the defect and stepped sites introduced by sputtering of the Co(0001) surface will result in a broad range of adsorption sites with varying (mostly less stable) adsorption energies.

DISCUSSION

As we have shown, the Co(111) and Co(0001) surfaces can be considered to behave the same toward hydrogen adsorption on the surface, and therefore, we will use the Co(111)/(0001) term to describe both surfaces together. The behavior found on the Co(111)/(0001) surface shows similarities with the adsorption and desorption of hydrogen on Ni(111), which was studied in great depth by Rendulic et al.[7,8] From the DFT

dx.doi.org/10.1021/cs2006586 | ACS Catal. 2012, 2, 1097−1107

Table 4. Zero-Point Energy Corrected Adsorption Energies (E_{ads}) and Estimated TPD Peak Temperatures ($\tilde{T}_{max}$) of Hydrogen on the Co(211) and Co(221) Stepped Surfaces

site[a]	E_{ads} [eV]	$\tilde{T}_{max}$[b] [K]	ν_i[c] [cm^{-1}]
Co(211)			
HH	−0.37	294	1134, 816, 802
Bf	−0.33	260	1102, 879, 743
4F	−0.32	252	855, 679, 434
2F	−0.43	335	1283, 1217, 189
Eh	−0.50	395	1155, 926, 630
Ef	−0.42	331	1155, 795, 783
Co(221)			
FH	−0.48	373	1157, 844, 818
HH	−0.44	343	1126, 814, 761
Bf	−0.33	267	1137, 908, 830
S	−0.30	237	950, 915, 644
Sf	−0.37	298	1141, 1058, 537
Ef	−0.55	432	1151, 1027, 702
Eh	−0.44	350	1125, 774, 718

[a]Site labels can be seen in Figure 9 [b]Estimated TPD peak temperature using the Redhead[37] equation. [c]Lists the calculated vibrational frequencies.

adsorption process profiles on Co(111) and the low initial sticking coefficients on Co(0001) (0.01−0.05), it is clear that the adsorption of hydrogen on a smooth Co(111)/(0001) surface is an activated process, as is the case on Ni(111) (reflected in the similarly low initial sticking coefficient of 0.05). Initially the β_2 state is populated on both Co(111)/(0001) and Ni(111), until a coverage of θ = 0.50 ML is reached. According to the DFT calculations, this will correspond to the hydrogen being adsorbed in either the hcp or fcc hollow sites on this surface. At around θ = 0.50 ML, the adsorption on Co(111)/(0001) becomes kinetically hindered due to the repulsion from the preadsorbed hydrogen atoms. On Ni, the β_1 state is populated after this, but this is associated with a sticking coefficient that is "exceedingly small".[8] On the fully covered Ni(111) surface (β_2 + β_1), a highly delocalized adsorption layer is proposed to exist due to lateral interactions. Our DFT results on Co(111) show that both the hcp and fcc sites remain likely adsorption sites at coverages above θ = 0.50 ML. It is also evident that lateral repulsions play a role on the Co(111)/(0001) surface, as can be seen in the decrease in adsorption strength with the increase in hydrogen coverage. The peak separations (β_2/β_1) in the TPD spectra of smooth Ni(111) and Co(0001) surfaces are the consequence of this repulsive lateral interaction between the hydrogen atoms.[7] The functional dependence of this coverage dependence on Co(111) shows a very strong resemblance to that shown on Ni(111), although this is not the case for the (100) facets of the two metals.[11] Another clear similarity between the Ni(111) and Co(111) surfaces is the high mobility of hydrogen atoms at low coverage in both cases.[40]

Defects were found to have a strong effect on adsorption and desorption behavior of hydrogen on both Ni and Co. The β_1 peak becomes prominent when a small amount of defects is present while the desorption temperature of the β_2 peak is not affected. Defects in the structure introduce sites where the adsorption process proceed with a significantly reduced adsorption barrier. The principle of microscopic reversibility dictates that recombination of hydrogen has the same barrier over and above the adsorption energy. Recombinant desorption over these sites would therefore be slightly easier as well. It must be noted that this effect cannot be very large since an adsorption barrier of only 0.08 eV has been calculated for the Co(111) surface (with multiple dynamic pathways possible, this single pathway barrier gives an estimate of the lower limit of the adsorption rate). Applying the Redhead equation to a decrease of 0.08 eV will correspond to a maximum decrease in TPD peak temperature of 28 K. We can see that upon introduction of defects the desorption peaks shifts are much larger. For a stepped or highly defected surface, the shift of the β_1 peak is ∼75 K lower, and the β_2 peak is shifted as well, by ∼20 K. The DFT analysis of hydrogen adsorption on stepped surface suggests that the introduction of defects introduces areas on the Co surface which have a variety of sites with differing coordination numbers. Many of these sites have weaker adsorption energies than that of the pure Co(111)/(0001) surface, giving rise to lower temperature features in the TPD trace. The effects of defects will thus depend on the amount of available defect sites.

We therefore interpret our experimental results found on Co(0001) in this way: adsorption of hydrogen is an activated process on smooth Co(0001), and defects offer an alternative channel for hydrogen adsorption/desorption without a barrier. This is first of all reflected in the sticking coefficient: it is much higher on both defected Co surfaces than on the smooth surface, clearly showing an enhancement of the sticking, which can be explained by the removal of the barrier associated with hydrogen adsorption on the smooth surface. The role of defects is also apparent in the shape of the desorption spectra. On Ni(111) the two desorption states (β_2 and β_1) could eventually be populated, although the sticking coefficient to populate the β_1 state is very low. On smooth Co(0001) population of the β_1 state does not occur, even after doses of 570 L or higher (not shown here). Population of the β_1 state on Co(0001) can only occur when enough defect sites are present, as seen on the slightly defected surface in our experiments. On the smooth surface, the θ = 0.5 ML hydrogen atoms completely inhibit hydrogen adsorption. On the slightly defected surface, the defect sites are still available for adsorption at an overall hydrogen coverage of θ = 0.5 ML, and the hydrogen concentration can continue to build up. Defects only start to play a significant role in the desorption temperature when their concentration is high, as in the case that the defect concentration is high enough for mostly all the hydrogen adsorption and recombination events to occur on a defect site. As a result the hydrogen desorption spectrum on the sputtered surface contains two very broad peaks, assigned to the β_1 and β_2 state, both shifted to significantly lower temperatures than on both the smooth and slightly defected surface. We conclude that, despite small differences, the hydrogen adsorption/desorption from Co is governed by similar principles as that on Ni.[7,8]

CONCLUSIONS

We have performed plane-wave DFT calculations with the GGA-PW91 method to calculate the coverage dependent adsorption properties of hydrogen on the 111 and 100 facets of FCC-Co. These values have been compared to calculations on the HCP-Co(0001) surface. Further calculations on the Co(211) and Co(221) surfaces have been performed to model the effects of step and defect sites. A microkinetic analysis of desorption, which incorporates coverage dependent adsorption energies, has been presented to simulate the

dx.doi.org/10.1021/cs2006586 | ACS Catal. 2012, 2, 1097−1107

expected TPD experiments. The DFT work was complemented by a TPD study of the adsorption and desorption of hydrogen on a smooth single crystal of Co(0001). The effect of defects has been studied by TPD after introduction of defects by sputtering of this Co surface. From these studies the following is concluded:

(a) The nature of hydrogen adsorption on the Co(111) and Co(0001) surfaces is similar. Hydrogen adsorbs dissociatively in the fcc and hcp hollow sites on the Co(111)/(0001) surface. At the low coverages of θ = 0.11 and 0.25 ML, the DFT adsorption energies are −0.48 eV/atom (0.96 eV/H_2 desorption) and −0.49 eV/atom (0.98 eV/H_2 desorption), respectively. These are in line with the values extracted from the TPD experiment (between 0.97 and 1.1 eV). Hydrogen atoms on this surface at low coverage will be very mobile having a diffusion barrier of only 0.12 eV. Experimental TPD results show that adsorption on a smooth Co(0001) surface proceeds with a sticking coefficient of between 0.01 and 0.05. The adsorption of hydrogen on a smooth Co(111)/(0001) is a slightly activated process. The adsorption energy of hydrogen on this surface is coverage dependent, showing a decrease around θ = 0.5 ML in the order of 0.12 eV. This is similar to what has been shown on Ni(111) and contrasts previous conclusions that hydrogen adsorption energies are coverage independent on Co.[12] Adsorption/desorption of hydrogen on Co is governed by mainly the same principles reported for Ni.

(b) On a smooth Co(111)/(0001) surface, the experimental adsorption saturation coverage is about θ_{max} = 0.5 ML, although DFT predicts $\theta_{max} \approx$ 1.0 ML. The origin of the discrepancy lies in the adsorption process, where the hydrogen already present on the surface will kinetically impede the adsorption of more hydrogen as the coverage approaches θ = 0.5 ML, due to an increase in the approach barrier of the H_2 molecule.

(c) Adsorption of hydrogen on the Co(100) surface is possible on both the bridge and hollow sites, with the hollow site taking preference. The adsorption of hydrogen is coverage independent up to θ = 1.00 ML, differing from observations on the Ni(100) surface. The low coverage adsorption energy is −0.46 eV, which is very similar in magnitude to the Co(111)/(0001) surface. The hydrogen atoms will also be very mobile on this surface.

(d) Simulated TPD traces generated from the DFT data indicated that on the Co(111) surface the coverage dependent adsorption energies result in two adsorption features, with the peak separation being 57 K, which is in very good agreement with our TPD experiments. On the Co(100) surface only one desorption feature is expected.

(e) As on the Ni(111) surfaces, defects play an important role in the adsorption process. Defect and stepped sites allow for a variety of adsorption sites with differing coordination and adsorption energies. The presence of defect sites accelerates the adsorption of hydrogen by providing alternative, almost barrierless pathways of adsorption. Calculations on model stepped surfaces indicate that the presence of steps and defects will expose a broad range of adsorption sites with varying (mostly less favorable) adsorption energies. At low defect concentrations, the defect sites facilitate hydrogen adsorption but do not change the low coverage adsorption energies. These sites make it possible to increase the coverage on the Co(111)/(0001) surface above θ = 0.50 ML.

(f) The presence of defect sites in a high concentration will give rise to adsorption sites with much lower desorption activation energies, resulting in broad low temperature features on the hydrogen TPD.

■ ASSOCIATED CONTENT

Supporting Information

More details on the partition functions used in the Microkinetic Analysis, the derivation of the relation between desorption temperature shifts and adsorption energy changes, the coverage dependent hydrogen adsorption structures on Co(111), Co(0001), and Co(100), and details of hydrogen adsorption on the Co(211) and Co(221) stepped surfaces, as well as the calculation of relative rates of adsorption for precovered hydrogen surfaces. This material is available free of charge via the Internet at http://pubs.acs.org/.

■ AUTHOR INFORMATION

Corresponding Author

*E-mail: pieter.vanhelden@sasol.com.

Notes

The authors declare no competing financial interest.

■ ACKNOWLEDGMENTS

We thank Prof. J. W. Niemantsverdriet and Dr. A. M. Saib for their part in making this work possible.

■ REFERENCES

(1) Dry, M. E. *Catal. Today* **2002**, *71*, 227.
(2) Bridge, M. E.; Comrie, C. M.; Lambert, R. M. *J. Catal.* **1979**, *58*, 28.
(3) Johansson, M.; Lytken, O.; Chorkendorff, I. *J. Chem. Phys.* **2008**, *128*, 034706.
(4) Lisowski, W. *Appl. Surf. Sci.* **1988**, *35*, 399.
(5) Lisowski, W. *Appl. Surf. Sci.* **1989**, *37*, 272.
(6) Habermehl-Ćwirzeń, K. M. E.; Kauraala, K.; Lahtinen, J. *Phys. Scr.* **2004**, *T108*, 28.
(7) Rendulic, K. D.; Winkler, A.; Steinrück, H. P. *Surf. Sci.* **1987**, *185*, 469.
(8) Rendulic, K. D. *Appl. Phys. A: Mater. Sci. Process.* **1988**, *47*, 55.
(9) Christmann, K.; Schober, O.; Ertl, G.; Neumann, M. *J. Phys. Chem.* **1974**, *60*, 4528.
(10) Seebauer, E.; Kong, A. C. F.; Schmidt, L. D. *Surf. Sci.* **1988**, *193*, 417.
(11) Zhdanov, V. P. *Surf. Sci. Rep.* **1991**, *12*, 183.
(12) Klinke, D. J., II; Broadbelt, L. J. *Surf. Sci.* **1999**, *429*, 169.
(13) Greeley, J.; Mavrikakis, M. *J. Phys. Chem. B* **2005**, *109*, 3460.
(14) Saib, A. M.; Claeys, M.; Van Steen, E. *Catal. Today* **2002**, *71*, 395.
(15) Kitakami, O.; Sato, H.; Shimada, Y.; Sato, F.; Tanaka, M. *Phys. Rev. B* **1997**, *56*, 13849.
(16) Weststrate, C. J.; Gericke, H. J.; Verhoeven, M. W. G. M.; Ciobica, I. M.; Saib, A. M.; Niemantsverdriet, J. W. *J. Phys. Chem. Lett.* **2010**, *1*, 1767.
(17) Lahtinen, J.; Vaari, J.; Kauraala, K. *Surf. Sci.* **1998**, *418*, 502.
(18) Habermehl-Ćwirzeń, K. M. E.; Lahtinen, J.; Hautojärvi, P. *Surf. Sci.* **2005**, *598*, 128.
(19) Kresse, G.; Hafner, J. *Phys. Rev. B* **1993**, *47*, 558.
(20) Kresse, G.; Furthmüller, J. *Phys. Rev. B* **1996**, *54*, 11169.
(21) Perdew, J. P.; Wang, Y. *Phys. Rev. B* **1992**, *45*, 13244.
(22) Methfessel, M.; Paxton, A. T. *Phys. Rev. B* **1989**, *40*, 3616.

(23) Monkhorst, H. J.; Pack, J. D. *Phys. Rev. B* **1976**, *13*, 5188.
(24) Murnaghan, F. D. *Proc. Natl. Acad. Sci.* **1944**, *30*, 244.
(25) Birch, F. *Phys. Rev.* **1947**, *71*, 809.
(26) Aschroft, N. W.; Mermin, N. D. *Solid State Physics*; Holt, Rinehart and Winston: New York, 1976.
(27) Mehl, M. J.; Papaconstantopoulos, D. A. *Phys. Rev. B* **1996**, *54*, 4519.
(28) West, A. R. *Basic Solid State Chemistry*, 2nd ed.; Wiley & Sons Ltd.: New York, 1999.
(29) Mattson, T. R.; Mattson, A. E. *Phys. Rev. B* **2002**, *66*, 214110 ; http://dft.sandia.gov/functionals/webcalculator.html.
(30) Lide, D., Kehiaian, H., Eds. *CRC Handbook of Thermophysical and Thermochemical Data*; CRC Press: Boca Raton, FL, 1994.
(31) Vincent, F.; Figlarz, M. *C. R. Hebd. Seances Acad. Sci.* **1967**, *264C*, 1270.
(32) Fujihisa, H.; Takemura, K. *Phys. Rev. B* **1996**, *54*, 5.
(33) Huber, K. P.; Herzberg, G. *Molecular Spectra and Molecular Structure 4: Constants of Diatomic Molecules*; Van Norstrand Reinhold. Co.: New York, 1979.
(34) Jónsson, H.; Mills, G.; Jacobsen, K. W. In *Classical and Quantum Dynamics in Condensed Phase Simulations*; Berne, B. J., Ciccotti, G., Coker, D. F., Eds.; World Scientific: Singapore, 1998; pp 385−404.
(35) Anslyn, E. V.; Dougherty, D. A. *Modern Physical Organic Chemistry*; University Science Books, 2006; pp 365−373.
(36) Truhlar, D. G.; Garrett, B. C.; Klippenstein, S. J. *J. Phys. Chem.* **1996**, *100*, 12771.
(37) Redhead, P. A. *Vacuum* **1962**, *12*, 203.
(38) Habenschaden, E.; Kuppers, J. *Surf. Sci.* **1984**, *138*, L147.
(39) Falconer, J. L.; Madix, R. J. *J. Catal.* **1977**, *48*, 262.
(40) Felter, T.; Stulen, R.; Koszykowski, M.; Gdowski, G.; Garrett, B. *J. Vac. Sci. Technol.* **1989**, *A 7*, 104.